AD-755 397

# A STUDY OF ELECTRON DENSITY DISTRIBUTION IN VISCOUS FLOWS

Henry G. Lew

General Electric Company

Prepared for:

Air Force Cambridge Research Laboratories

November 1972

DISTRIBUTED BY:

NTIS

National Technical Information Service
U. S. DEPARTMENT OF COMMERCE
5285 Port Royal Road, Springfield Va. 22151

DOCUMENT NO. 72SD2189

AFCRL-72-0718

AD755397

# A STUDY OF ELECTRON DENSITY DISTRIBUTION IN VISCOUS FLOWS

by

Henry G. Lew

GENERAL ELECTRIC COMPANY
VALLEY FORGE, PENNSYLVANIA 19101

Contract No. F19628-72-C-0070
Project No. 4642
Task No. 464202
Work Unit No. 46420201

DDC
RECEIVED
FEB 13 1973
C

SCIENTIFIC REPORT NO. 1

NOVEMBER 1972

Approved for public release; distribution unlimited.

Contract Monitor: John F. Lennon
Microwave Physics Laboratory

Prepared for

AIR FORCE CAMBRIDGE RESEARCH LABORATORIES
AIR FORCE SYSTEMS COMMAND
UNITED STATES AIR FORCE
BEDFORD, MASSACHUSETTS 01730

Reproduced by
NATIONAL TECHNICAL
INFORMATION SERVICE
U S Department of Commerce
Springfield VA 22151

ACCESSION for
NTIS White Section
DDC Buff Section
UNANNOUNCED
JUSTIFICATION .....
.....
BY .....
DISTRIBUTION/AVAILABILITY CODES
Dist. AVAIL. and/or SPECIAL
A

Qualified requestors may obtain additional copies from the Defense Documentation Center. All others should apply to the National Technical Information Service.

UNCLASSIFIED
Security Classification

**DOCUMENT CONTROL DATA - R & D**
(Security classification of title, body of abstract and indexing annotation must be entered when the overall report is classified)

| | |
|---|---|
| 1. ORIGINATING ACTIVITY (Corporate author)<br>General Electric Company<br>Re-entry & Environmental Systems Div.<br>Valley Forge, Pennsylvania 19101 | 2a. REPORT SECURITY CLASSIFICATION<br>Unclassified<br>2b. GROUP |

3. REPORT TITLE

A STUDY OF ELECTRON DENSITY DISTRIBUTION IN VISCOUS FLOWS

4. DESCRIPTIVE NOTES (Type of report and inclusive dates)

Scientific - - Interim

5. AUTHOR(S) (First name, middle initial, last name)

Henry G. Lew

| | | |
|---|---|---|
| 6. REPORT DATE<br>November 1972 | 7a. TOTAL NO. OF PAGES<br>~~48~~ 62 | 7b. NO. OF REFS<br>16 |
| 8a. CONTRACT OR GRANT NO.<br>F19628-72-C-0070<br>b. PROJECT, TASK, AND WORK UNIT NO.<br>4642-02-01<br>c. DOD ELEMENT<br>62101F<br>d. DOD SUBELEMENT 684642 | 9a. ORIGINATOR'S REPORT NUMBER(S)<br>GE TIS 72SD2189<br>Scientific Report No. 1<br>9b. OTHER REPORT NO(S) (Any other numbers that may be assigned this report)<br>AFCRL-72-0718 | |

10. DISTRIBUTION STATEMENT

A - Approved for public release; distribution unlimited.

| | |
|---|---|
| 11. SUPPLEMENTARY NOTES<br>TECH, OTHER | 12. SPONSORING MILITARY ACTIVITY<br>Air Force Cambridge Research Laboratories (LZ)<br>L. G. Hamscom Field<br>Bedford, Massachusetts 01730 |

13. ABSTRACT

The electron production for the viscous flow over a body in hypersonic flight and high altitudes has been studied and predictions of its magnitude have been made. The flight parameters selected for this study were typical of those encountered by the reentry nosecone experiments launched in a series of Air Force Cambridge Research Laboratories/Trailblazer II Rocket Flights. A chemical system appropriate for high temperature dissociated and ionized air has been utilized. In addition to $NO^+$ the chemical kinetic system includes $N_2^+$, $O_2^+$, $O^+$, $N^+$. Both chemical and nonequilibrium effects are included. An evaluation of various wall conditions such as catalyticity and slip, of diffusion coefficients, and of magnitudes of various rate constants has also been considered. Results of electron density distribution have been obtained for flow at the stagnation region and along the Trailblazer II body. Comparison of these predictions with the AFCRL experimental flight data shows good agreement[12,13].

DD FORM 1 NOV 65 1473

I

UNCLASSIFIED
Security Classification

UNCLASSIFIED

Security Classification

| 14 KEY WORDS | LINK A ROLE | LINK A WT | LINK B ROLE | LINK B WT | LINK C ROLE | LINK C WT |
|---|---|---|---|---|---|---|
| Ionized Flow, Viscous Shock Layer, Boundary Layer, Electron Density, Blunt Body Flow Field | | | | | | |

II

UNCLASSIFIED

Security Classification

DOCUMENT NO. 72SD2189

AFCRL-72-0718

# A STUDY OF ELECTRON DENSITY DISTRIBUTION IN VISCOUS FLOWS


by

Henry G. Lew

GENERAL ELECTRIC COMPANY
VALLEY FORGE, PENNSYLVANIA 19101



Contract No. F19628-72-C-0070
Project No. 4642
Task No. 464202
Work Unit No. 46420201

SCIENTIFIC REPORT NO. 1

NOVEMBER 1972


Approved for public release; distribution unlimited.

Contract Monitor: John F. Lennon
Microwave Physics Laboratory

Prepared for

AIR FORCE CAMBRIDGE RESEARCH LABORATORIES
AIR FORCE SYSTEMS COMMAND
UNITED STATES AIR FORCE
BEDFORD, MASSACHUSETTS 01730

III

TABLE OF CONTENTS


| | | Page |
|---|---|---|
| I. | INTRODUCTION | 1 |
| II. | CHEMICAL KINETIC RATE CONSTANTS | 2 |
| III. | VIBRATIONAL NONEQUILIBRIUM EFFECT | 4 |
| | 3.1 Vibrational Relaxation Model | |
| | 3.2 Typical Results for the Distribution of Characteristics in the Viscous Layer | |
| IV. | EFFECT OF VARIOUS PHENOMENA ON THE ELECTRON DENSITY PRODUCTION. | 13 |
| | 4.1 Wall Catalyticity | |
| | 4.2 Slip Effects at the Wall | |
| | 4.3 Effect of Diffusion Coefficients | |
| | 4.4 Effect of Transverse Step Size | |
| | 4.5 Effect of Chemical Kinetic Rate Constants on the Formation of Electrons | |
| | 4.6 Variation of Electron Density Along the Body | |
| V. | CONCLUDING REMARKS | 21 |
| VI. | REFERENCES | 23 |
| VII. | TABLES | 25 |
| VIII. | LIST OF FIGURES, FIGURES 1-15 | 31 |

# I. INTRODUCTION

The electron production in the viscous layer over blunt bodies in hypersonic flight is dependent on the energy exchanges within the flow and its aerodynamic flight configuration. For a non-ablating body the reaction between high temperature dissociated air species which requires the least energy to produce an electron is the associative ionization of the nitrogen and oxygen atoms. With increasing temperatures collisional ionization of these species begins to make a contribution to the net number of electrons. Thus the determination of the electron density over bodies in hypersonic flight is influenced by the vehicle shape, the thermodynamics of the flight regime, and the energy distribution in the various internal modes of the gaseous molecules.

The purpose of this report is to predict the electron density distribution over a blunt $9^{o}$ sphere-cone body (Figure 1) typical of the AFCRL Trailblazer II vehicle. The report is a continuation of the study of Reference 1. In that reference a discussion of the method utilized for the prediction of electron density was given together with results for several altitude-velocity regimes. This report considers the physical phenomena (to be discussed subsequently) of importance to the electron production and makes further predictions of flow fields at different altitude-velocity regimes. The salient features of the predictions are given herein; the detail distributions of velocity, temperature, species concentration and in particular, the electron density are given in separate documents of Reference 2.

## II. CHEMICAL KINETIC RATE CONSTANTS

The chemical kinetics system for a nitrogen-oxygen atmosphere is of concern in this study. The flight regime involves principally velocities to 17,500 ft/sec. Since there is no ablation of body material the gas mixture is composed of dissociated and ionized air species. For most cases these species are $O_2$, $N_2$, N, O, NO, $NO^+$ and electrons. To cover the conditions involving the higher temperature range to 15,000°K and the altitude range to 100 km the additional atomic and molecular ions of $N_2^+$, $O_2^+$, $N^+$, and $O^+$ are included. The chemical system involving the neutral species and $NO^+$ is given in reactions 1 to 6 in Table I which also contains additional reactions which become important at the higher temperature range of 15,000°K. This Table of reactions has been suggested by Bortner[3] for a nitrogen-oxygen system typical of the shock layer of re-entry bodies. At the higher temperatures the associative ionization reactions 7 and 8 and collisional ionization reactions for the neutral species as given by 9 to 13 become important. Finally, after the formation of the positive ions, exchange reactions redistribute these charges by means of reactions 14 to 20. The reaction rate constants have been suggested by Bortner in Reference (4) and (5) where he also discusses their uncertainties and limitations. Results in this report are obtained using reactions 1-6 and reactions 1-10, 14, 15, 17, 18, 20. A minimum number of reactions consistent with reality is utilized.

In general, the chemical reactions are represented by the equation

$$\sum_{i=1}^{N} \alpha_{ri} X_i \rightleftharpoons \sum_{i=1}^{N} \beta_{ri} X_i \qquad (1)$$

where the subscript r represents the particular reaction, i is the species that is being reacted and $\alpha_{ri}$, $\beta_{ri}$ are the stoichiometric coefficients. In this report the values of r and i range over the number of reactions and the number of species respectively. For this representation the net mass rate of production of species i per unit volume can be immediately given by

$$w_i = M_i \sum_{r=1}^{R} (\beta_{ri} - \alpha_{ri}) \left[ k_{fr} \prod_{j=1}^{J} \left( \frac{\rho c_j}{M_j} \right)^{\alpha_{rj}} - k_{br} \prod_{j=1}^{J} \left( \frac{\rho c_j}{M_j} \right)^{\beta_{rj}} \right] \qquad (2)$$

In this equation $M_i$ is the molecular weight of species i and the subscript j denotes the species and the catalytic bodies, i.e., j = 1, 2, ... N, N+1, ... J. The mass fraction of catalytic bodies is given in terms of the N species by

$$c_j = M_j \sum_{i=1}^{J} Z_{(j-N),i} c_i / M_i \qquad (3)$$

for j = N+1, .... J. The use of equation (3) facilitates the computation problem for large systems of chemical species and flow variables.

Equation (2) is the source term for the mass generation of species and is a function of the density $\rho$ of the mixture, the temperature T, and the density ($\rho c_i$) of the pertinent species. The rate constants $k_{fr}$ and $k_{br}$ are, of course, functions of the temperature T.

## III. VIBRATIONAL NONEQUILIBRIUM EFFECT

The excitation of the molecular constituents at hypersonic speed is a complex phenomenon. Energy is transferred by collision and is distributed among the different modes at different times which are comparable to the flight time, i.e., the relaxation times for vibrational and rotational modes are different from those for translation. Translational energy is rapidly absorbed first with the rotational mode requiring only a few additional collisions. In most cases at the higher velocities and densities the vibrational mode rapidly becomes equilibrated prior to the initiation of the ionization reactions. At intermediate values of densities and temperatures this vibrational equilibrium time is of the order of the chemical time. In this case the vibrational relaxation process has a significant effect on the electron production. Any change in the electron density caused by a lag in the vibrational mode depends on the interaction of an increase in the kinetic temperature since the heat capacity has not achieved its equilibium value and a decrease of the dissociation rate of the molecular species; thus the electrons are decreased (or increased) since their production depends mostly on the dissociation of the molecular species except at the very high temperatures. At the high temperature prevalent at the altitudes and flight velocity considered the electron density is very sensitive to a small change in temperature.

### 3.1 Vibrational Relaxation Model

It has been known for some time that the chemical relaxation of the flow after excitation by the bow shock is affected to an appreciable extent by the state of the vibrational modes[6,7,8]. The dissociation of the molecular

species depends largely on the population of vibrational levels and the probability of dissociation from each of the individual levels. There is a coupling between the vibrational relaxation and the dissociation process which has shown to be important by Hammerling, Teare, and Kivel[7]. The effect of dissociation on vibrational relaxation has been studied by Treanor and Marrone first[8] for equal probability of dissociation from any vibrational level and then for an assumed probability distribution which has higher probability for dissociation from the higher levels[6]. By adjusting a parameter which they called the characteristic probability temperature, good agreement was found with experimental values of dissociation lag time and rate constants[6]. In this model the relaxation of the vibrational modes occurs through a series of Boltzmann population distributions until equilibrium is reached. The principal effect of this coupled vibration-dissociation is the reduction of the dissociation rate constant from its value at vibrational equilibrium. This, of course, reduces the formation of atomic species. And consequently, the production of electrons from associative ionization of O and N atoms.

In the present study the relaxation of the diatomic species $O_2$ and $N_2$ by collision with O, N, $O_2$ and $N_2$ is examined. The average energy per molecule obtained by summing over the vibrational levels of the molecules is given by

$$E = \sum_{i=1}^{i_{max}} \left(E_i \frac{n_i}{n}\right) \tag{4}$$

where $n_i$ and n are the $i^{th}$ level and total number densities respectively. $E_i$

is the energy at the $i^{th}$ level. In the consideration herein four collision partners of $O_2$, $N_2$, O, and N are allowed and both molecular species $O_2$ and $N_2$ are vibrationally relaxing. The relaxation equation for the energy as defined by Equation (4) is then given by

$$u \frac{dE}{ds} = \frac{E_\infty - E}{\tau_v} - \frac{[E_f - E]}{n} \left(\frac{dn}{dt}\right)_f + \frac{[E_r - E]}{n} \left(\frac{dn}{dt}\right)_r \tag{5}$$

where n is the number density of the dissociating molecules, $\tau_v$ is the relaxation time, $(dn/dt)_f$ and $(dn/dt)_r$ are the rate of dissociation and recombination of the molecule and u the velocity along the streamlines. The quantities $E_f$ and $E_r$ are the average vibrational energy per molecule lost in dissociation or gained in recombination respectively. $E_f$ is a function of the translational and vibrational temperatures while the energy lost to recombination is a function of the translational temperature. The energy at equilibrium $E_\infty$ is achieved when the vibrational temperature becomes equal to the translational temperature. Its difference from the instantaneous value of E is the driving function for the relaxing Landau-Teller model.

By defining a quantity $T_F$ given by

$$\frac{1}{T_F} = \frac{1}{T_v} - \frac{1}{T} - \frac{1}{U} \tag{6}$$

where $T_v$ and T are the vibrational and translation temperatures respectively, the energy terms can be written as

$$E_f = \frac{1}{Q(T_F)} \sum_j E_j \exp\left[- E_j/kT_F\right] \tag{7a}$$

$$E_r = \frac{1}{Q(-U)} \sum_i E_i \exp\left[-E_i/kU\right] \tag{7b}$$

where the Q's are the partition functions of the respective arguments, and as before $E_i$ is the energy of the vibrational levels, and U will be given in terms of the ratio of the dissociation energy D and the Boltzmann constant k.

The parameter U has values that are adjustable and determines the probability of dissociation for each of the vibrational levels. For very large values of U there is equal probability of dissociation from all vibrational levels[5]. For preferential dissociation from the higher levels, values of $U = D/3k$ and $D/6k$ have been used[3] together with a choice of vibrational relaxation times so that the dissociation rate constants are in agreement with experiment. These values of U have led to a $T^{-2}$ pre-exponential dependence of the rate constant which is too large an exponent on the basis of experiment data. The larger values of $U = \infty$ give a $T^{-1}$ dependence which is closer to the value suggested by Bortner[4] on the basis of measurement. However, the value of $U = \infty$ does not lead to values of the dissociation lag time comparable to the experimental values of Wray[9] although the preferential model does lead to reasonable values of the dissociation incubation time[6]. Values of the coupling factor which is the ratio of the actual dissociation rate to that at vibrational equilibrium are almost independent of temperature in the range greater than $6000^{\circ}K$ for the preferential model which has lower values than the non-preferential model. On the basis of a steady state analysis[10] where the vibrational population distribution which is non-Boltzmann, the assumption of $U = 3T$ is needed to give a coupling factor with almost no dependence on temperature. Thus there is

some choice in the value of U to be utilized. In this study, U is kept as a parameter with values suggested by normal shock experimental data which can be changed as required by comparison with the experimental flight data.

In the vibrational model for both the $O_2$ and $N_2$ molecules (with collision partners of the principal air species $O_2$, $N_2$, O and N), the relaxation time is required. Millikan and White[4] have derived an empirical relaxation time-pressure relation as a function of translational temperature for various systems of gases. This has been given in the form

$$\ln_e (p\tau_v) = (1.16 \times 10^{-13})\, \mu^{\frac{1}{2}} \theta^{\frac{4}{3}} \left( T^{-\frac{1}{3}} - .015^{\frac{1}{4}} \right) - 18.42 \qquad (8)$$

where $(p\tau_v)$ is the product of the gas pressure in atmospheres and the relaxation time $\tau_v$ in sec., T is $^{o}$K in this equation, $\mu$ the reduced mass $(M_i M_j)/(M_i + M_j)$, $\theta$ is the vibrational constant $h\nu/k$, and p is in units of atmospheres. The range of validity of Equation (8) extends over values of $\mu$ for the air species although temperature extrapolation is necessary to reach 12,000$^{o}$K which prevails at the shock front.

The molecular constants used for $O_2$ and $N_2$ are given in Table II.

The vibrational relaxation time is inversely proportional to the pressure within the shock layer; this is evident from Equation (8). Values of the time are shown on Figure 2 for the conditions from .003 atm to 0.1 atm which bounds the stagnation pressure between 270,000 ft. down to 200,000 ft. altitude for the

flight velocity of 17,500 ft/sec. Characteristic flow time in the shock layer is of the order of $10^{-5}$ sec at 270,000 ft. altitude in the stagnation region. This can be compared with the vibrational relaxation time of Figure 2. One notes that the characteristic time at the stagnation region can be simply given by the relation

$$t_{char} = \int \frac{dy}{v} \tag{9}$$

where y and v are the coordinate and velocity normal to the body surface respectively and the integration limits are over the fraction of the shock layer where the characteristic time is desired.

The net dissociation and recombination from a molecular species is the sum of the reactions occurring at each vibrational level. In terms of the population distribution these rates are

$$\left.\begin{aligned} k_{fr} &= \sum_{i=0}^{i_{max}} \frac{n_i}{n} k_{fr}^{i} \\ k_{br} &= \sum_{i=0}^{i_{max}} k_{br}^{i} \end{aligned}\right\} \tag{10}$$

where $(n_i/n)$ is a Boltzmann distribution defined in terms of the vibrational temperature $T_v$. The summation is over all the vibrational levels. The probability[8] of dissociation from level i is defined as

$$p_i = \frac{1}{Q(T_F)} \exp\left[-E_i/kT_F\right] \tag{11}$$

and furthermore, since $k_{fr}^{i}$ is independent of $T_v$, the dissociation rate constant is given by

$$k_{fr} = X\, k_{fr/eq}. \tag{12}$$

The equation is in terms of the vibrational equilibrium rate constant and X is given by

$$X = \frac{Q(T)}{Q(T_v)} \frac{\sum_i \exp\left[-E_i/kT_F\right]}{\sum_i \exp\left[E_i/kU\right]} \tag{13}$$

This function gives directly the effect of the vibration-dissociation coupling on the rate constant. In fact, this leads to one effect on the flow field electron density production since the chemical rate constants are depressed from the value at vibrational equilibrium. A second one is the increase of kinetic temperature at vibrational nonequilibrium.

In the above equation the energy levels of the oscillators must be assigned. Experimental data can be used to define the energy levels. The partition function Q can be then simply written for the harmonic oscillator in the form

$$Q = \frac{\exp\left(-E_{10}N/kT\right) - 1}{\exp\left(-E_{10}/kT\right) - 1} \tag{14}$$

where N is the number of levels of the oscillator, and $E_{10} = h\nu$ is the

vibrational constant. The constants for the $O_2$ and $N_2$ oscillators utilized in this report are given in Table II.

### 3.2 Typical Results for the Distributions of Characteristics in the Viscous Layer

The vibrational nonequilibrium equations together with the flow equations and chemical source have been coupled together and solved simultaneously by a finite difference method utilizing iteration to account for the many nonlinearities of the system. High altitude considerations utilizing the shock slip conditions account for the finite thickness of the shockwave. These equations, as mentioned before, have been given in a prior report[1]. Consider the flow at 240,000 ft. altitude for a body flight velocity of 17,500 ft/sec. The Reynolds number at the stagnation region is small[1] and the entire flow region in the nose region is viscous. This can be seen from the velocity curve on Figure 3; there is no sharp demarcation of slope. The velocity curve on Figure 3 also shows the effect of shock slip. (The temperature was not normalized by the Rankine-Hugoniot value.) The species distributions are denoted by the corresponding name on Figures 3 and 4. Peak values of both oxygen and nitrogen atoms occur at about 5 mm distance away from the body whereas nitric oxide peaks at about 2 mm. The peak temperature occurs near the edge of the layer where the dissociation of molecular oxygen is also maximum. Thus convection of the dissociated species from the edge together with diffusion leads to the distribution shown on Figure 4. Correspondingly, the electron production maximizes near the outer edge of the layer whereas the electron density peaks nearer the body surface (at about 2.6 mm from the surface of Figure 5). There are three

temperatures in the viscous layer and these are the kinetic temperature and the vibrational temperatures of the oxygen and nitrogen molecules. The distributions of these temperatures are shown on Figure 6. The vibrational temperature of the oxygen molecules rises rapidly near the shock front and approaches the kinetic temperature near the wall. Of particular significance here is the fact that vibrational nonequilibrium occurs through most of the shock layer thickness so that the reaction rate constants do not have their full equilibrium values and there is a correspondingly higher kinetic temperature than for the vibrational equilibrium case. The electron density production is changed in opposite directions by these two effects; the effect that dominates the electron density is dependent on the altitude. The change in electron density with altitude is shown on Figure 7. It is important to note that the vibrational nonequilibrium effects on electron density is contained principally in the altitudes shown therein. This is an example of typical results; additional ones are contained in the report[2] referenced previously and in the 1970 report[1]. Figure 7 shows that between the altitudes shown the electron density for the vibrationally nonequilibrium flow is higher than that for vibrational equilibrium with a cross-over at about 270,000 ft. altitude. The principal phenomena controlling these distributions are the dissociation of the oxygen molecule and the magnitude of the kinetic temperature which is dependent on the degree of vibrational equilibrium. Near the altitude of 270,000 ft. the dissociation rate of oxygen molecules for vibrational equilibrium is higher than that for vibrationally nonequilibrium despite the higher kinetic temperature.

## IV. EFFECT OF VARIOUS PHENOMENA ON THE ELECTRON DENSITY PRODUCTION

There are a number of factors that can influence the magnitude of the electron density. Considerations are given to them in this Section.

### 4.1 Wall Catalyticity

The wall temperature at the high altitudes considered in this Report is low and it is expected that the dissociated species recombine in the gas phase to their molecular constituents. Experimental measurements of gas radiation appear to indicate that nitric oxide has a non-zero value near the surface to account for the magnitude observed. If this is the case then the electron density is increased from that of a fully catalytic surface. The non-catalytic condition for species is given by the vanishing of the mass flux

$$\dot{m}_i = 0 \tag{15}$$

where i denotes the species. Since there is no mass transfer at the body surface Equation (15) implies a similar condition on the diffusion flux.

Consider the non-catalytic wall condition for the nitric oxide concentration only. There are no atomic species at the wall. The electron density distribution has been obtained with this condition for the altitude-velocity of 270,000 ft. - 17,500 ft/sec for vibrational equilibrium. A 9.1% increase in peak electron density over the case with a fully catalytic wall condition was obtained. A comparison of electron density changes due to this condition together with other effects are shown on Table III.

It would be of interest to compare the electron density for the two extremes of wall conditions and these are a fully catalytic one and a non-catalytic one for all species. Of course, at the low wall temperature concerned, it is expected that the former condition would be more typical for heat sink body material. For the non-catalytic wall for all the species there are non-zero values of the atomic species in addition to those of nitric oxide. The results for the 240,000 ft. altitude and 17,500 ft/sec velocity case (vibrational equilibrium) show that the nitric oxide and its ion, and the nitrogen atom concentrations (mass fraction) still peak within the layer but the other species do not. However, since the mass density increases toward the wall the electron density achieves its maximum there. The electron density distributions for both wall conditions are compared on Figure 8. The peak values differ by an order of magnitude as expected. As pointed out before it is likely that the wall condition is non-catalytic for all species. Air Force Cambridge Research Labs. experimental flight data [Rotman[12], Hayes[13]] appear to indicate that the electron density increases away from the surface at least for streamwise points along the body away from the stagnation region. It is noted that the fully catalytic wall conditions for atomic species also lead to the same type of variation. Thus the fully non-catalytic wall condition would certainly give the maximum electron density obtainable as far as recombination wall effects are concerned.

## 4.2 Slip Effects at the Wall

Gas molecules exchange energy and momentum with the surface of the body by means of collision. Since there are velocity and temperature differences between the gas and the body surface, momentum and energy are transferred bet-

ween them. When the gas molecules do not attain the momentum and energy corresponding to the conditions at the boundary in a single collison then there exists a velocity slip and a lack of complete accommodation between the gas and the wall. Thus velocity and temperature jumps occur at the solid boundary over a distance of the mean free path of the gas. In a gas with high density (low altitude flight) these effects are not important, they only become important in the high altitude regime. The effects of slip and the lack of accommodation result in discontinuities of the tangential velocity and the temperature and are given for the velocity u and temperature T by relations[14,15]

$$u(0) = \frac{2-\sigma}{\sigma} \bar{L} \left(\frac{\partial u}{\partial y}\right)_o \tag{16a}$$

$$T(0) - T_w = \frac{2-\alpha}{\alpha} \cdot \frac{2\gamma}{\gamma+1} \frac{\bar{L}}{P_r} \left(\frac{\partial T}{\partial y}\right)_o \tag{16b}$$

where the coefficients multiplying the derivatives on the right side of Equations (16a, 16b) are known as the slip coefficient and the temperature jump coefficient respectively. In addition, $\bar{L}$ denote the local mean free path of the gas and becomes small for high density, $\gamma$ the isentropic constant, $\sigma$ is the fraction of diffusely reflected molecules whose average tangential velocity is zero, $\alpha$ is the accommodation coefficient (temperature), and $P_r$ is the local Prandtl number. It is seen that the jumps are proportional to the mean free path of the gas. Equations (16a and b) are derived from semi-macroscopic agreement usually for a monatomic gas; Equation (16b) is written in the form valid for a polyatomic gas.

Recent examination[16] of the temperature jump in a polyatomic gas shows that the values of the temperature jump are always slightly less than those for monatomic gases. The two coefficients $\sigma$ and $\alpha$ are prescribed constants and are close to unity. For example, $\alpha$ vary from .87 to .97[14] for aluminum. The values were taken to be unity for the numerical results given in this report. It is seen from Equations (16a and b) that both the velocity derivatives are positive for a cool wall. This fact implies that there are positive jumps in both velocity and temperature which are inversely proportional to the ambient air density.

An evaluation of this effect has been made for the (270,000 ft;17,500 ft/sec) condition. At the wall the velocity ratio has jumped to .03147 from the zero value. The temperature in the gas at the wall has increased by a factor of 1.9 of the body temperature. This has the consequence of increasing the magnitude of the temperature distribution (Figure 9) and therefore the concentration of atomic species. The net increase in the peak number density of electrons for this case is only 1.7% and is small. Although the temperature near the body surface has increased sufficiently to noticeably influence the ionization rate there, most of the electrons are produced principally near the outer two-thirds part of the layer and hence the peak electrons are not noticeably changed. Near the wall the concentration of nitric oxide ion is increased by the higher temperature due to the jump; however, the electron number density is decreased by 21% due to the fact that the density is decreased by the temperature jump.

Since the jumps of velocity and temperature are proportional to their derivatives and mean free path their variation around the body requires further evaluation.

### 4.3 Effect of Diffusion Coefficient

Diffusion has a considerable influence in distributing the electrons produced in the high temperature region near the shock front. This fact has been pointed out in a previous paragraph. The results given in this report have been obtained for a constant Lewis number (= $\rho D_{ij}\bar{C}_p/k$ where $\rho$ is the mass density, $D_{ij}$ the binary diffusion coefficient, $\bar{C}_p$ the mixture specific heat at constant pressure, and k the coefficient of heat conductivity) in which $\rho$, $\bar{C}_p$, and k are computed for each point as a function of the mixture concentration and temperature. Comparisons have shown that the assumption of a constant Lewis number is a valid representation for a multi-component diffusion providing there are no large disparate species masses. Thus dissociated air species satisfy this requirement; an example in which it is not satisfied is a hydrogen-air mixture.

A Lewis number of 1.4 has been utilized in all the results considered in this report except as noted differently. To demonstrate the effect of diffusion numerical results for the case (270,000 ft;17,500 ft/sec) have been obtained with the Lewis number equaled to 1.6. The peak electron density decreases by 17.5% due to increasing the diffusion coefficient. That is, there is a higher spread of the electrons produced.

## 4.4 Effect of Transverse Step Size on Electron Density Near Wall

Since there are flight measurements which are close to the surface of the body the nonlinear variation in that region is of particular interest. This point was investigated by decreasing the uniform step size and by the use of a coordinate transformation which created a nonuniform step size normal to the wall with a smaller step size near the wall as required. With use of the transformation the second order accuracy in the finite difference scheme was retained. The independent variable $\eta$ transverse to the wall is transformed to the $\zeta$ coordinate by the function

$$\zeta = \eta_{max} \left[ 1 + \frac{\tanh\left(\alpha\left(\frac{\eta}{\eta_{max}} - 1\right)\right)}{\tanh \alpha} \right] \tag{17}$$

where $\alpha$ is a constant to be assigned. This constant is used to adjust the step size near the wall. Smaller values of $\alpha$ will lead to higher concentration of increments near the wall. The equations of motion as given in Reference (1) were transformed to the new coordinate and modifications were made accordingly.

An example of the electron density variation for different step sizes is shown on Figure 10.

## 4.5 Effect of Chemical Rate Constants on the Formation of Electrons

It was pointed out in Section II that at the higher temperatures and low density additional ionization mechanisms may assume some importance in the production of electrons. Consideration is given in this section to the behavior

of the electron density for different chemical rate constants. A first example is the flight condition at the highest altitude (270,000 ft) which has a translational temperature near the shock front of about 9630°K. It is noted tha all shock layer temperatures for flight conditions between the altitude 200,000 ft. and 270,000 ft. for the velocity 17,500 ft/sec are below 11,500°K. Most values of the temperatures are below 10,000°K except for the one case at 200,000 ft. altitude. Results for the (270,000 ft;17,500 ft/sec) case with the additional ionization mechanisms given by reactions 1-10, 14, 15, 17, 18, and 20 of Table I were obtained. With these reactions the species of $N_2^+$, $O_2^+$, $O^+$, $N^+$ are added to the other air species. The peak electron density is increased by a factor of 5 with the additional reactions and species. A comparison of the distribution of electrons between the 6 species and 10 species cases is given on Figure 11. There are now five positive ions generated within the flow. Of particular interest is that $NO^+$ and $O_2^+$ are almost equal and are larger by one to two orders of magnitude than the $N^+$ and $O^+$ ions. This difference is shown on Figure 12. Although the electron density has not changed appreciably the dominant ion now is $O_2^+$. Most of the concentration of $O_2^+$ ion is produced near the shock front and the production rate at this point is higher than that of $NO^+$ by an order of magnitude.

A study was also made on the effect of changing the various reaction rate constants on the production of electrons for 6 species. The dissociation rate of oxygen molecules (reaction 1) was increased by an order of magnitude for the (240,000 ft. alt; 17,500 ft/sec) vibrational equilibrium case and resulted in

producing more atoms as expected. The peak temperature was decreased by about 12% and resulted in a 34% decrease in the peak electron density. It may have been expected that the increase in oxygen atoms would result in a higher electron density but as it is seen the dominant factor here is the temperature. Thus the flow field variables clearly can not be uncoupled from the species production.

In order to determine the effect of the deionization rate of reaction 6 its rate constant was lowered by one order from the value given in Table I. This resulted in a small increase in the electron density of 2.5% for the vibrational equilibrium (240,000 ft;17,500 ft/sec) case. Thus the electron density distribution has not been changed appreciably by this rate constant. The electron density distributions are shown on Figure 11.

## 4.6 Variation of Electron Density Along the Body

The entire distribution of electron density for vibrational equilibrium (270,000 ft;17,500 ft/sec) over the body has been considered utilizing the method reported in Reference (1) for six species and the chemical reactions 1-6 on Table I. Two sets of typical variations of electron density, velocity ratio, and temperature ratio are shown on Figure (13) and (14) for the two locations at 6.6 cm and 76.45 cm along the surface measured from the stagnation point. It is seen that the temperature peak develops within the viscous layer back along the body as expected for blunt conical bodies. The peak electron density along the body is shown on Figure (15); the maximum occurs near the stagnation region and decays toward the local equilibrium value.

## V. CONCLUDING REMARKS

The electron density for the viscous flow over a body in hypersonic flight and high altitudes has been studied in the report. A number of phenomena which can influence the production of electrons has been quantitatively evaluated. These include the effect of vibrational relaxation of the oxygen and nitrogen molecules, wall catalyticity, slip effects at the wall, magnitude of the diffusion coefficients, magnitude of the chemical kinetic rate constants, chemical kinetic mechanisms at high temperature, and transverse step size within the flow field. The principal conclusions can be summarized as follows:

1. Vibrational nonequilibrium effects cause higher electron density between 200,000 ft. and slightly below 270,000 ft. altitudes for the flight velocity of 17,500 ft/sec.

2. The non-catalytic wall condition for nitric oxide increases the electron density. Non-catalytic condition for all species causes the largest increase of electron density over that of a fully catalytic wall.

3. Slip effects at the wall due to the fact that the energy and momentum transferred between the gas and wall are not accomplished in a single collision are localized near the wall. There is an increase in the $NO^+$ concentration but a large decrease in electron density near the wall due to the temperature jump. Further study is required to determine its effect along the body and its effect on the additional positive ions at the higher temperature.

4. Larger diffusion coefficient lowers the peak electron density and distributes the electrons to all parts of the layer. Within the spread of Lewis number of 1.4 and 1.6 there is a 17.5% decrease.

5. The nonlinear variation of electron density at the wall has been obtained for small step sizes.

6. Chemical kinetic mechanisms and rates for the inclusion of the nitrogen and oxygen molecular and atomic ions which are present at the higher temperatures have been considered for a total of 10 species and 15 reactions. One case of (270,000 ft. alt;17,500 ft/sec) at the stagnation region has been considered and the peak electron density has been increased by a factor of 5 from that of the 6 species model.

7. The effect of increasing the dissociation rate of oxygen decreases the peak electron density even though the atomic oxygen has been increased. The reason is that the temperature has been lowered.

8. An order of magnitude change of the deionization rate of the nitric oxide ion has only a small effect on the electron density.

These results have been obtained from the study of a number of cases limited to the stagnation region. An evaluation of the electron density at other conditions at the stagnation region and at points around the body will add further information.

Detailed numerical results are given in separate documents of Reference (2).

## VI. REFERENCES


1. Lew, H. G., "Shock Layer Ionization at High Altitude", AFCRL 70-0702 & 70SD872), November 1970.

2. Lew, H. G., "Hypersonic Viscous Shock Layer Ionization at High Altitude", Data Memos A, 1, 2, 3, 1972 issued by GE to AFCRL, 1971-72.

3. Bortner, M., private communication.

4. Bortner, M., "A Review of Data Constants of Selected Reactions of Interest in Re-entry Flow Fields in the Atmosphere", National Bureau of Standards Technical Note 484, May 1969.

5. Bortner, M. (ed.), DASA Reaction Rate Handbook, Defense Atomic Support Agency Information and Analysis Center, October 1967.

6 Marrone, P. and Treanor, C., "Chemical Relaxation with Preferential Dissociation from Excited Vibrational Levels", Physics of Fluid, Vol. 6, No. 9, September 1963.

7. Hammerling, P., Teare, J. D., and Kivel, B., "Theory of Radiation from Luminous Shock Waves in Nitrogen", Physics of Fluid, Vol. 2, No. 4, 1959.

8. Treanor, C. and Marrone, P., "Effect of Dissociation on the Rate of Vibrational Relaxation", Physics of Fluid, Vol. 5, No. 9, 1022-1026, 1962.

9. Wray, K., "Shock Tube Study of the Coupling of the $O_2$-Ar Rates of Dissociation and Vibrational Relaxation", Journ. of Chem. Phys., Vol. 37, 1254-1263, 1962.

10. Treanor, C., "Coupling of Vibration and Dissociation in Gas Dynamic Flows", AIAA Paper No. 65-29, 1965.

11. Millikan, R., and White, D., "Systematics of Vibrational Relaxation", Journal of Chemical Physics, Vol. 39, No. 12, 1963.

12. Rotman, W., "Microwave Measurements of Flow Field Characteristics at the Stagnation Point of a Blunt Re-entry Body", AIAA Paper No. 72-693, AIAA 5th Fluid and Plasma Dynamics Conference, June 1972.

13. Hayes, D. T., "Electrostatic Probe Measurements of Flow Field Characteristics of a Blunt Body Re-entry Vehicle", AIAA Paper No. 72-694, AIAA 5th Fluid and Plasma Dynamics Conference, June 1972.

14. Schaaf, S., and Chambre, P., "Flow of Rarefied Gases in Fundamentals of Gas Dynamics", High Speed Aerodynamics and Jet Propulsion, Vol. III, Princeton, 1958.

15. Street, R. E., "A Study of Boundary Conditions in Slip-Flow Aerodynamics", Proceedings of First International Symposium of Rarefield Gas Dynamics, Pergammon Press, 1960.

16. Lin, J. T., "Kinetic Theory Analysis of Temperature Jump in a Polyatomic Gas", University of California, Berkeley Report No. AS-70-6, June 1970

## VII. TABLES

I. Chemical System of Air Reactions and Rates

II. Molecular Constants

III. Peak Electron Density Changes for Various Conditions

TABLE I

CHEMICAL SYSTEM OF AIR REACTIONS AND RATES

| REACTIONS | FORWARD | | | BACKWARD | | |
|---|---|---|---|---|---|---|
| | a | b | c | a | b | c |
| 1. $O_2 + M_1 = 2O + M_1$ | 8.74 (17) | -1 | .594 (5) | 7.26 (14) | - .5 | 0 |
| 2. $N_2 + M_2 = 2N + M_2$ | 2.41 (18) | - .8 | .1132 (6) | 1.34 (17) | - .8 | 0 |
| 3. $NO + M_3 = O + N + M_3$ | 1.45 (16) | 0 | .754 (5) | 3.63 (15) | 0 | 0 |
| 4. $O + NO = N + O_2$ | 4.33 (7) | 1.5 | .181 (5) | 1.81 (8) | 1.5 | .3 (4) |
| 5. $O + N_2 = N + NO$ | 6.02 (12) | 0 | .38 (5) | 1.32 (13) | 0 | 0 |
| 6. $O + N = NO^+ + e$ | 5.18 (11) | 0 | .319 (5) | 1.44 (21) | -1.5 | 0 |
| 7. $N + N = N_2^+ + e$ | 4.7 (8) | 1.3 | .678 (5) | 5.3 (17) | - .2 | 0 |
| 8. $O + O = O_2^+ + e$ | 6.62 (7) | 1.3 | .807 (5) | 7.22 (18) | - .7 | 0 |
| 9. $N + M = N^+ + e + M$ | 1.81 (19) | -1. | .169 (6) | 1.09 (27) | -2.5 | 0 |
| 10. $O + M = O^+ + e + M$ | 3.01 (18) | -1. | .158 (6) | 7.25 (26) | -2.5 | 0 |
| 11. $N_2 + M = N_2^+ + e + M$ | 1.81 (4) | 2 | .181 (6) | 1.09 (12) | .5 | 0 |
| 12. $O_2 + M = O_2^+ + e + M$ | 6.02 (3) | 1.5 | .14 (6) | 5.8 (11) | 0 | 0 |
| 13. $NO + M = NO^+ + e + M$ | 6.02 (17) | -1. | .1079 (6) | 3.63 (26) | -2.5 | 0 |
| 14. $N_2^+ + O_2 = N_2 + O_2^+$ | 1.20 (14) | 0 | 0 | 3.61 (13) | 0 | .409 (5) |
| 15. $N_2^+ + O = NO^+ + N$ | 1.51 (14) | 0 | 0 | 2.71 (14) | 0 | .354 (5) |

TABLE I

CHEMICAL SYSTEM OF AIR REACTIONS AND RATES (Continued)

| REACTIONS | FORWARD | | | BACKWARD | | |
|---|---|---|---|---|---|---|
| | a | b | c | a | b | c |
| 16. $N^+ + O_2 = NO^+ + O$ | 3.01 (14) | 0 | 0 | 6.02 (12) | .5 | .872 (5) |
| 17. $N^+ + NO = N + NO^+$ | 4.82 (14) | 0 | 0 | 2.11 (14) | .5 | .492 (5) |
| 18. $O^+ + N_2 = NO^+ + N$ | 6.02 (11) | 0 | 0 | 1.81 (11) | 0 | .124 (5) |
| 19. $O^+ + O_2 = O + O_2$ | 1.2 (13) | 0 | 0 | 1.81 (12) | 0 | .179 (5) |
| 20. $O_2^+ + NO = O_2 + NO^+$ | 4.82 (14) | 0 | 0 | 2.53 (14) | 0 | .322 (5) |

$k = aT^b \exp(-c/T)$, moles, sec, $^oK$, cm

$N(x) = N^x$

TABLE I

CHEMICAL SYSTEM OF AIR REACTIONS AND RATES (Continued)

Third Body Efficiencies

| Species | $M_1$ | $M_2$ | $M_3$ | $M_4$ |
|---|---|---|---|---|
| $O_2$ | 25 | 1 | 1.1 | 1 |
| $N_2$ | 25 | 3.24 | 1.1 | 1 |
| O | 105 | 1 | 50 | 1 |
| N | 1 | 21.6 | 50 | 1 |
| NO | 1 | 1 | 50 | 1 |

## TABLE II

MOLECULAR CONSTANTS

| Species | $E_{10} = h\nu$ ERGS | Dissociation Energy, $D/k^{o}K$ | Levels* (N) |
|---|---|---|---|
| $O_2$ | $3.1409655 \times 10^{-13}$ | 59400 | 26 |
| $N_2$ | $4.5897248 \times 10^{-13}$ | 113200 | 34 |

$k = 1.38 \times 10^{-16}$ Ergs/$^{o}$K, Boltzmann Constant

$h = 6.625 \times 10^{-27}$ Ergs sec, Planck's Constant

$\nu$ = frequency

* Cut-off Harmonic Oscillator

TABLE III

PEAK ELECTRON DENSITY CHANGE FOR VARIOUS CONDITIONS

| Condition | Percent Change in Peak Electron Density |
|---|---|
| Nitric Oxide - Noncatalytic | +9.1 |
| Non-catalytic - All Species | +600 |
| Wall Slip | +1.7 (Electron density near the wall is decreased by 21%) |
| Additional Ionized Species | +500 |
| Increase Oxygen Dissociation Rate - One Order | -34. |
| Decrease Deionization Rate (Reaction 6) by One Order | +2.5 |

## LIST OF FIGURES


1. Coordinate System and Body Geometry

2. Vibrational Relaxation Time of $O_2$

3. Vibrational Nonequilibrium Distributions of Velocity, Temperature, and Species Concentration in Mass Fractions at Stagnation Region, 240,000 ft; 17,500 ft/sec

4. Species Concentration in Mass Fraction at Stagnation Region for Vibrational Nonequilibrium, 240,000 ft;17,500 ft/sec

5. Electron Density ($cc^{-1}$) for Vibrational Nonequilibrium at the Stagnation Region, 240,000 ft;17,500 ft/sec

6. Kinetic and Vibrational Temperature ($^{o}K$) Distributions for Vibrational Nonequilibrium Flow at the Stagnation Region, 240,000 ft;17,500 ft/sec

7. Peak Electron Density Variation with Altitude at the Stagnation Region for the Velocity of 17,500 ft/sec

8. Electron Density Profiles for Catalytic and Non-Catalytic Walls at the Stagnation Region, 240,000 ft;17,500 ft/sec

9. Effect of Wall Slip on the Temperature Distribution at the Stagnation Region, 270,000 ft;17,500 ft/sec

10. Effect of Step Size on the Distribution of Electron Density at the Stagnation Region for Vibrational Nonequilibrium, 240,000 ft;17,500 ft/sec

11. Electron Density Distributions at the Stagnation Region for 6 Species ($NO^+$) and 10 Species ($NO^+$, $N_2^+$, $O_2^+$, $N^+$, $O^+$) at 270,000 ft and 17,500 ft/sec

12. Ion Concentration at the Stagnation Region at 270,000 ft and 17,500 ft/sec

13. Temperature, Velocity, and Electron Density Profiles for the Sphere Cone Trailblazer Body at $x = .066$ meter, 270,000 ft;17,500 ft/sec

14. Temperature, Velocity, and Electron Density Profiles for the Sphere Cone Trailblazer Body at $x = .066$ meter, 270,000 ft;17,500 ft/sec

15. Peak Electron Density Decay Along the Body of Trailblazer at 270,000 ft and 17,500 ft/sec

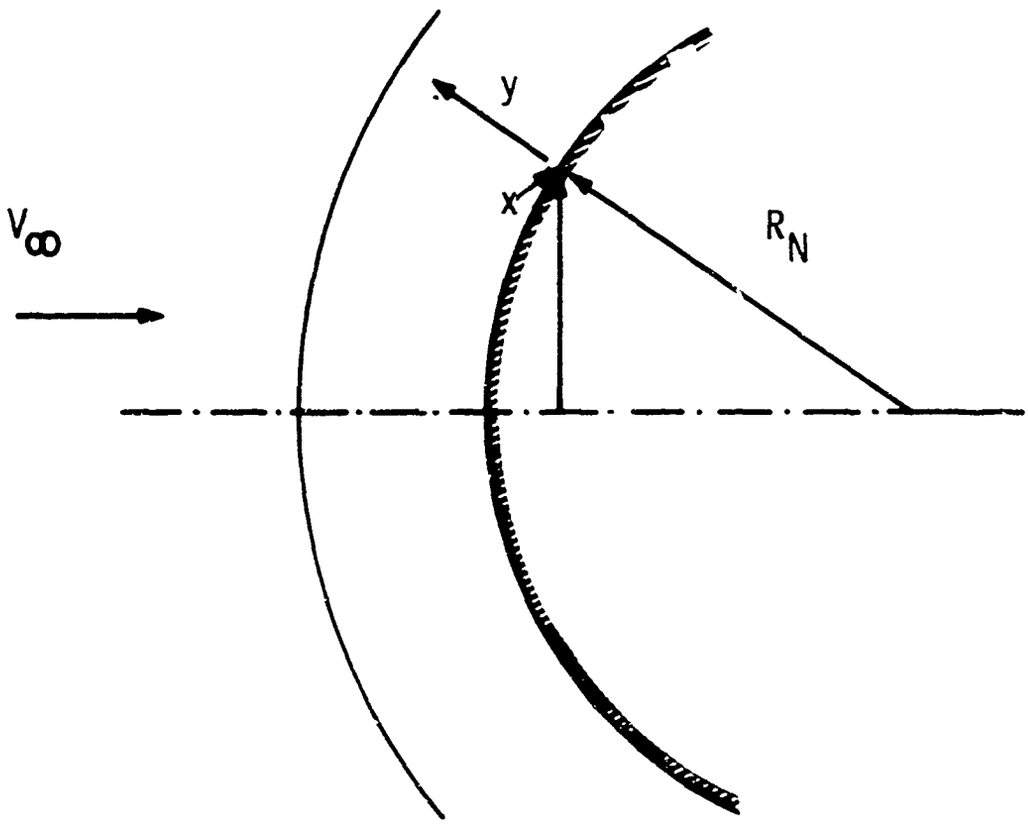


Figure 1. Coordinate System and Body Geometry

LEW N 209-507

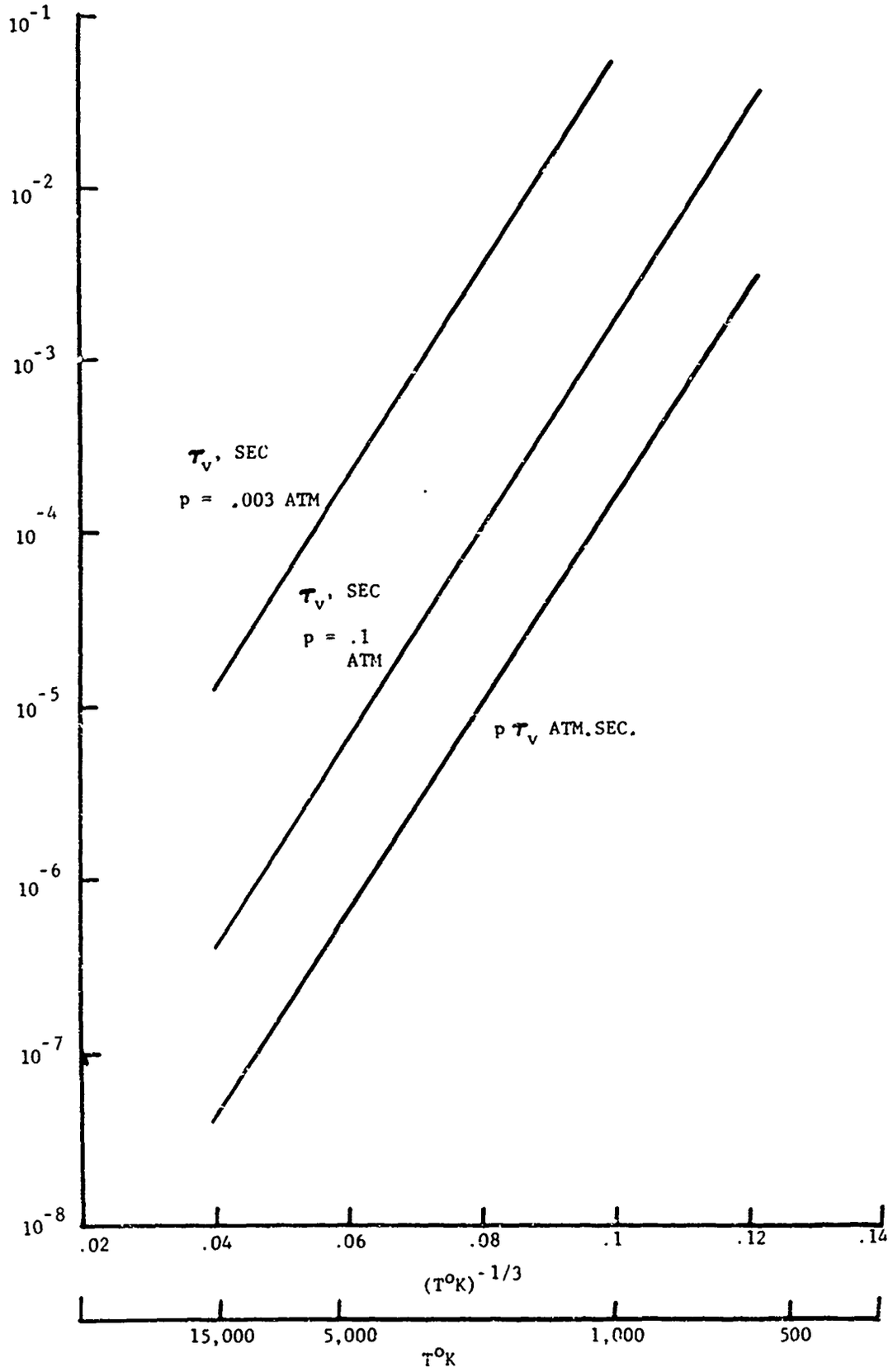


Figure 2. Vibrational Relaxation Time of $O_2$

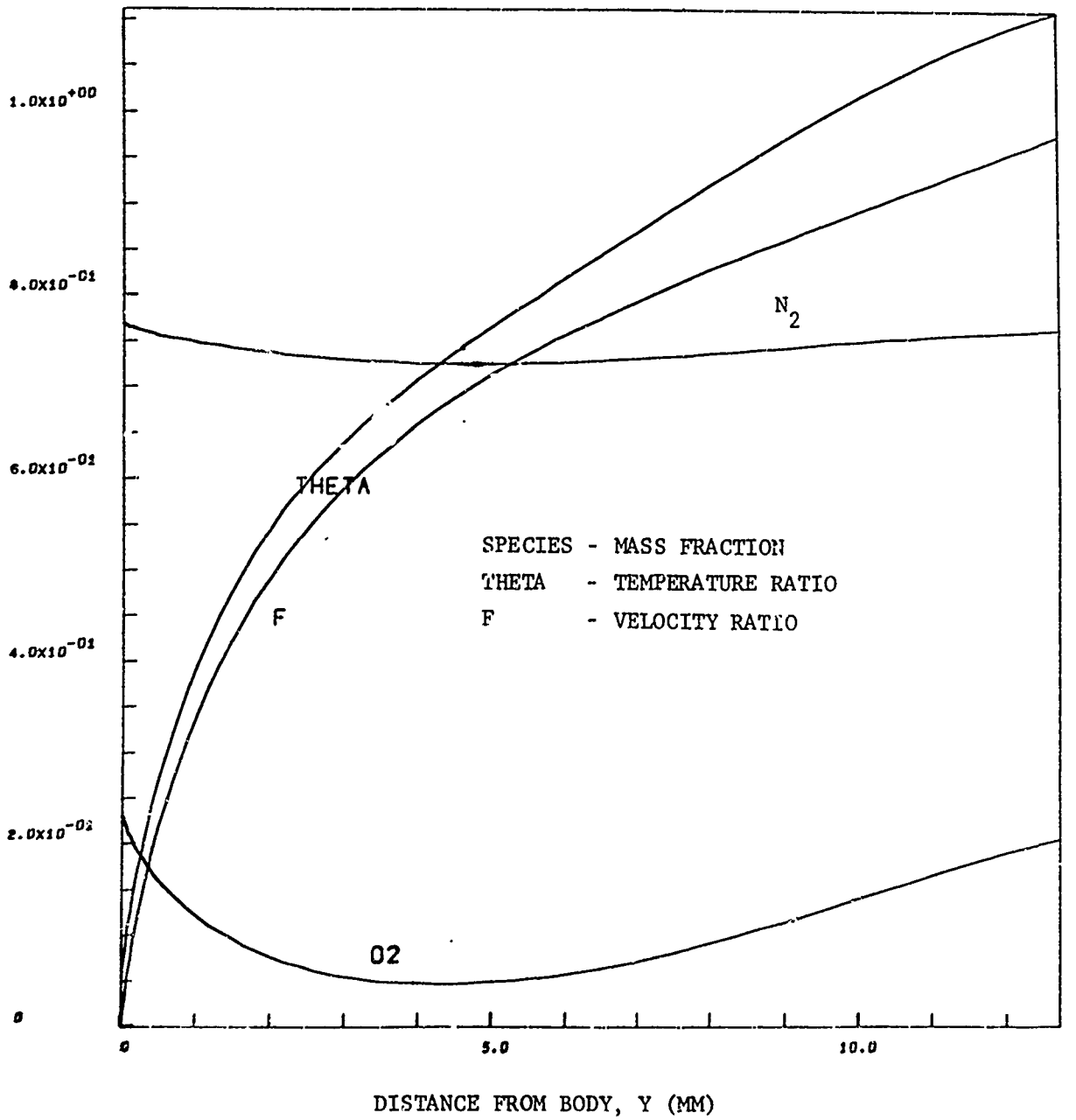


Figure 3. Vibrational Nonequilibrium Distributions of Velocity, Temperature, and Species Concentration in Mass Fraction at Stagnation Region, 240,000 ft; 17,500 ft/sec

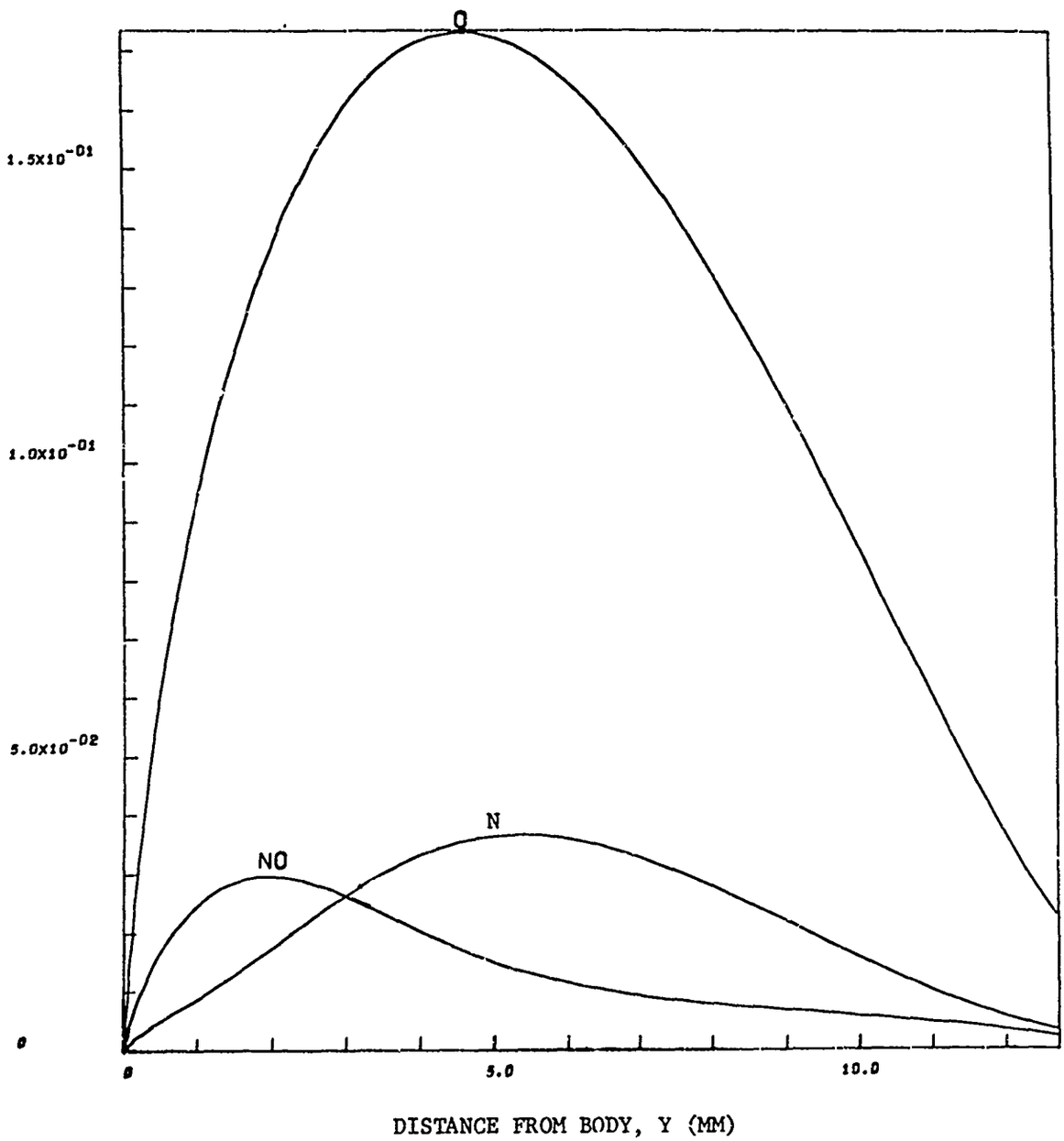


Figure 4. Species Concentration in Mass Fraction at Stagnation Region for Vibrational Nonequilibrium, 240,000 ft; 17,500 ft/sec

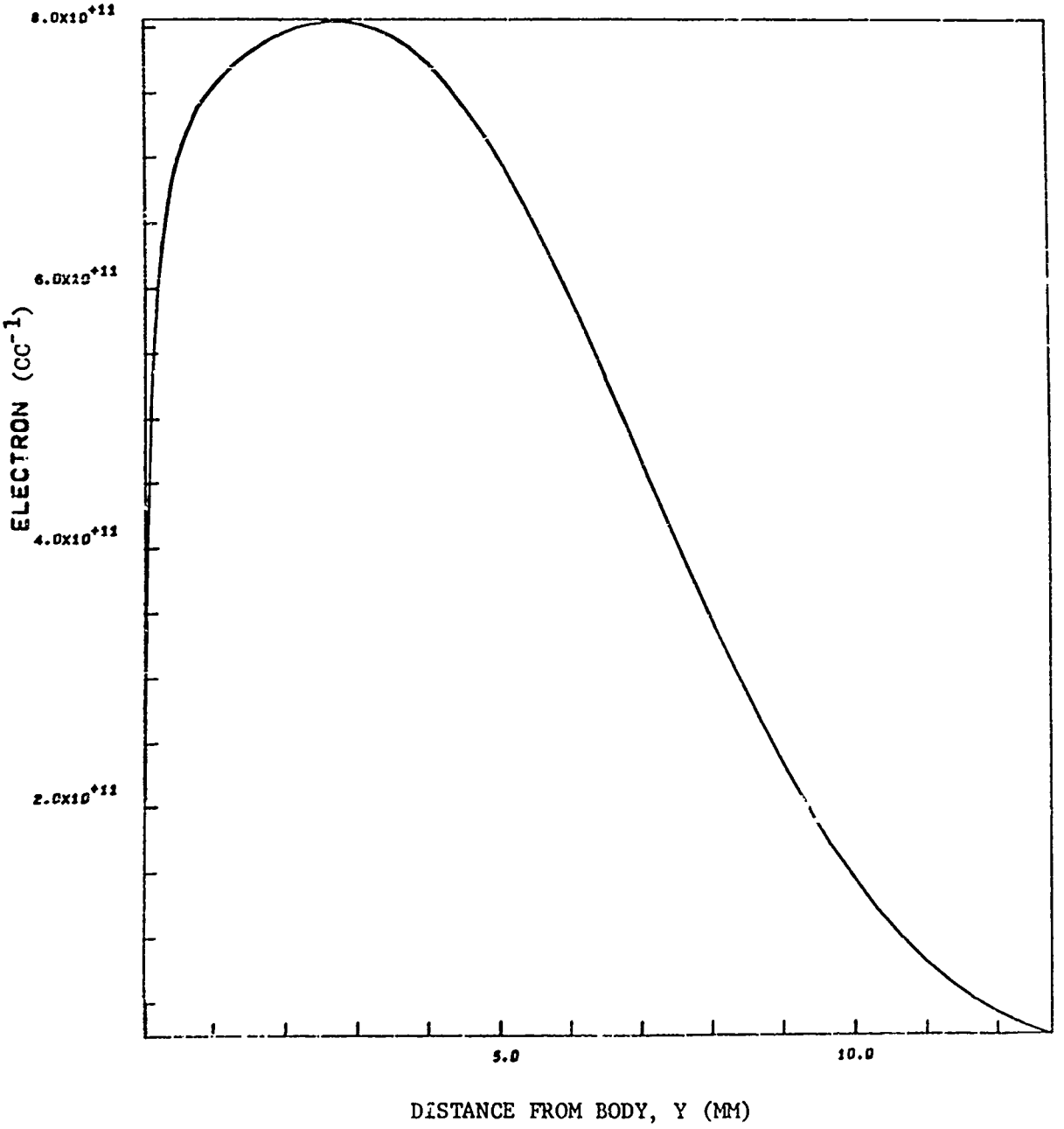


Figure 5. Electron Density ($CC^{-1}$) for Vibrational Nonequilibrium at the Stagnation Region, 240,000; 17,500 ft/sec

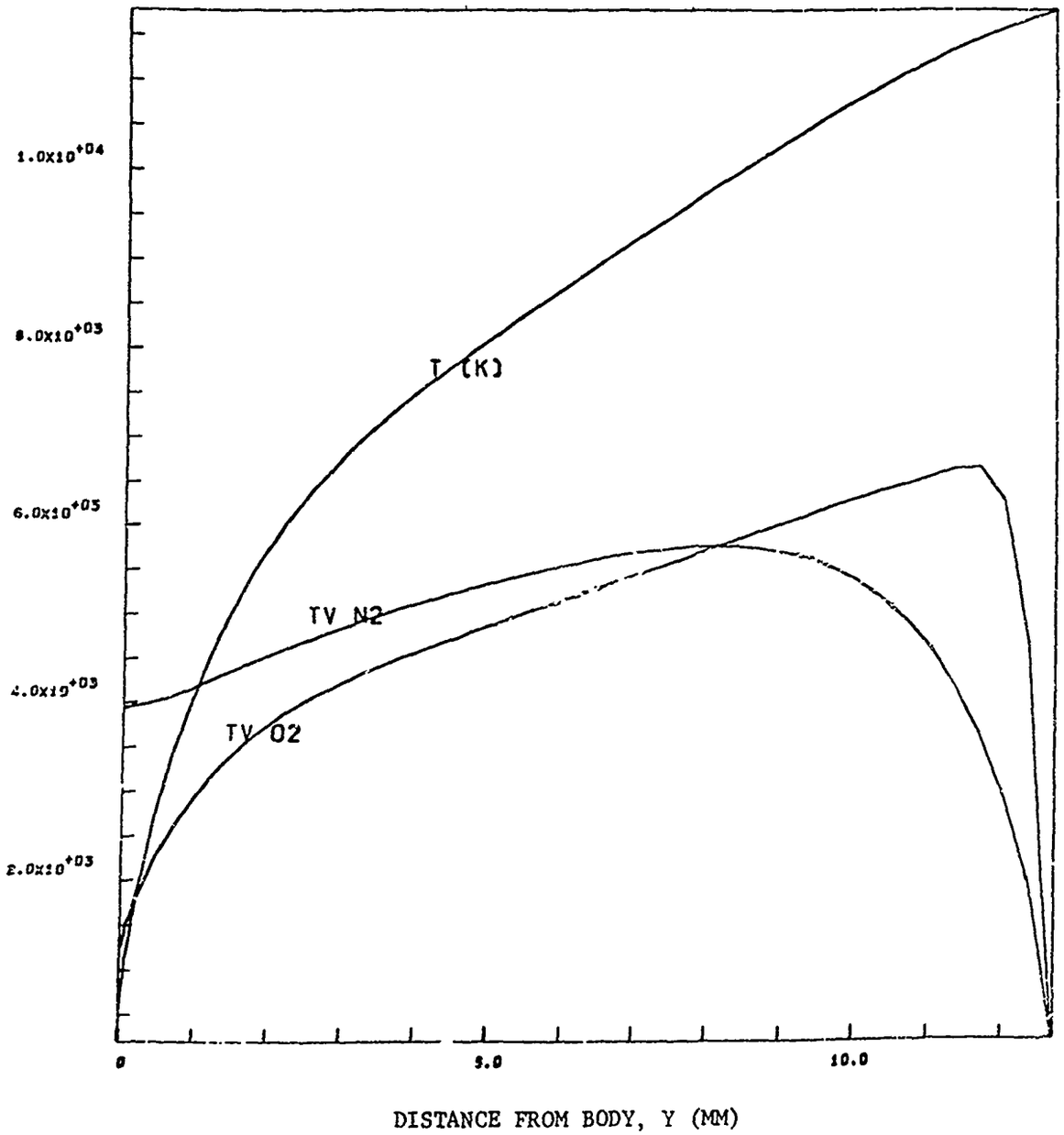


Figure 6. Kinetic and Vibrational Temperature ($^{o}K$) Distributions for Vibrational Nonequilibrium Flow at the Stagnation Region, 270,000 ft; 17,500 ft/sec

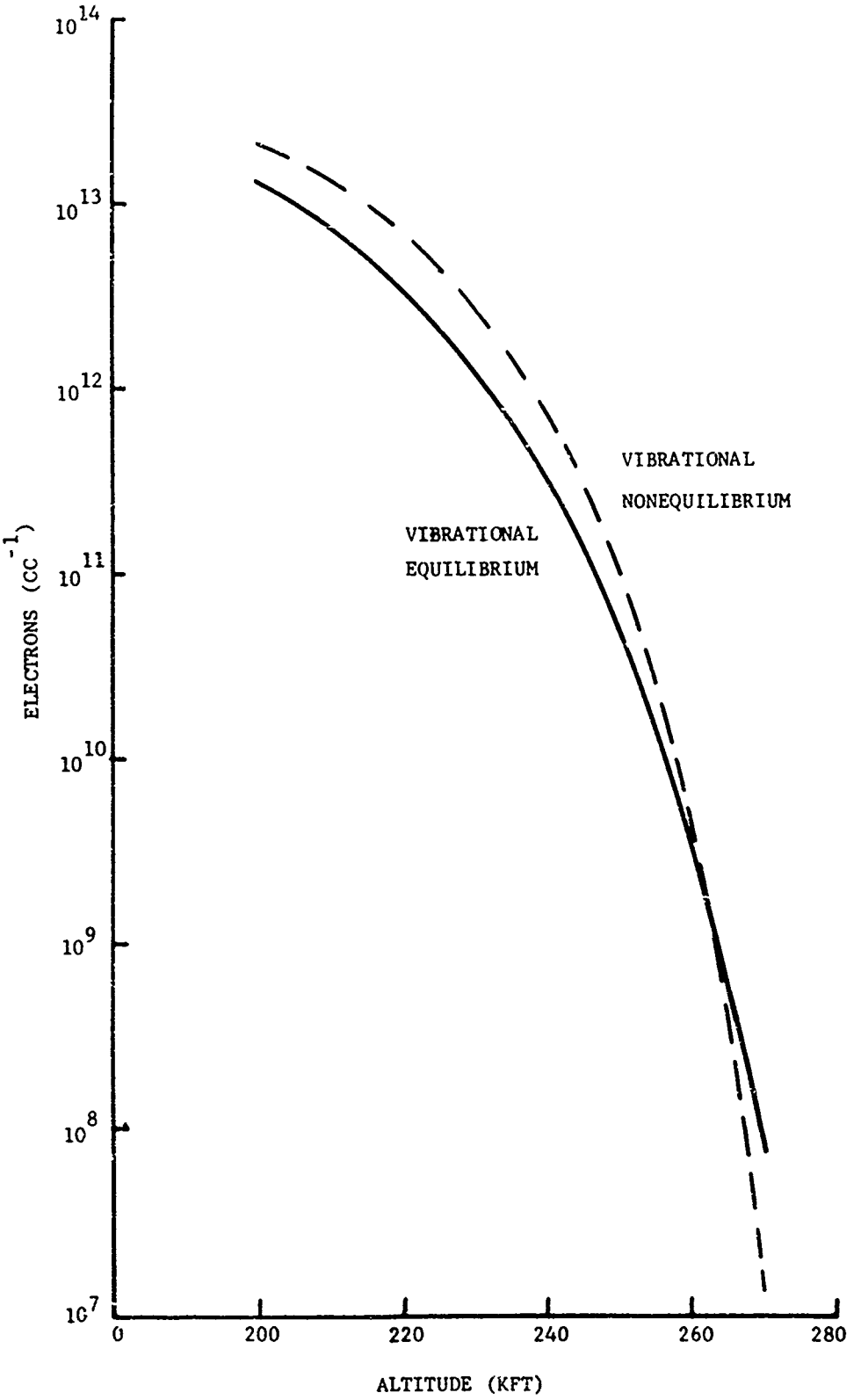


Figure 7. Peak Electron Density Variation with Altitude at the Stagnation Region for the Velocity of 17,500 ft/sec

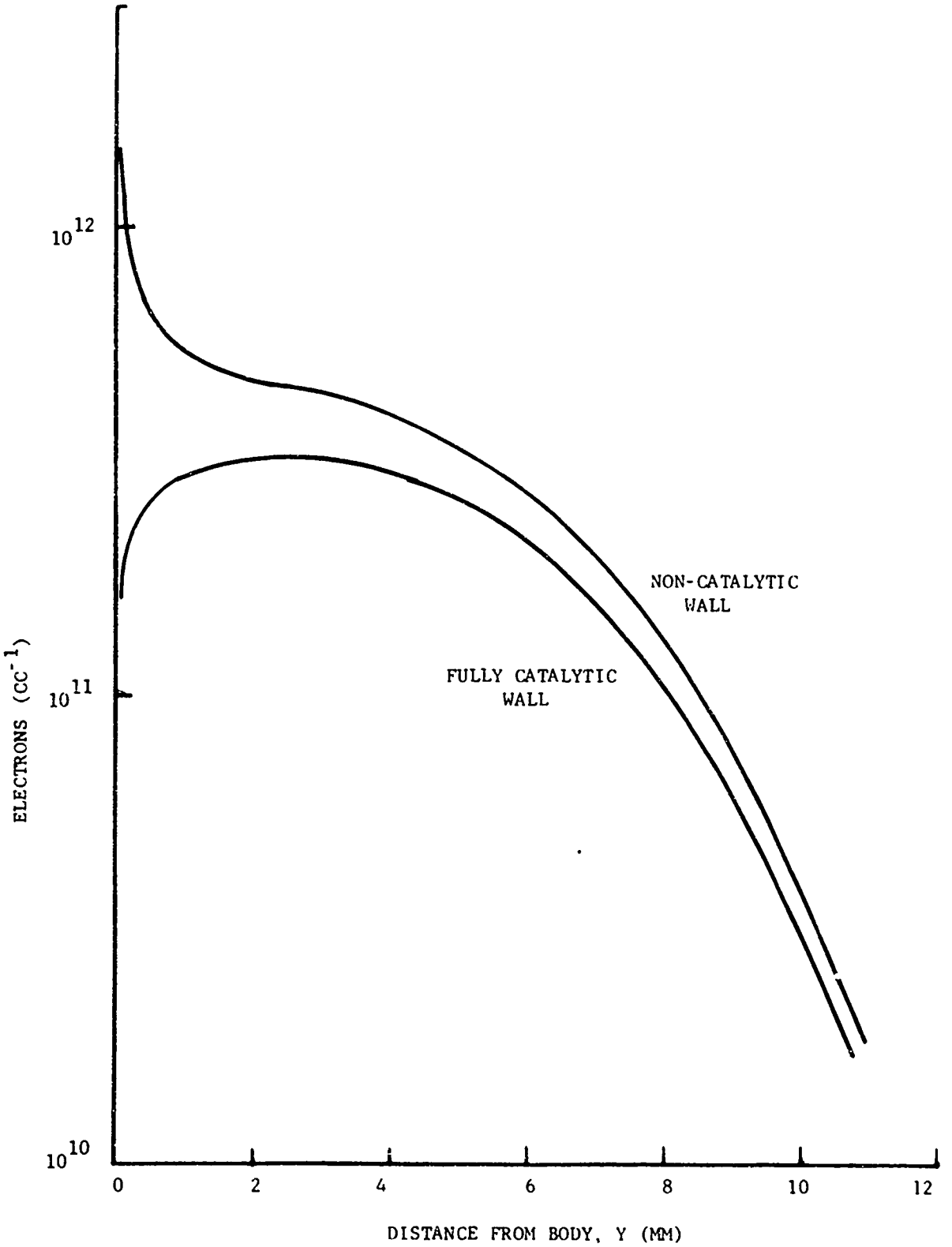


Figure 8. Electron Density Profiles for Catalytic and Non-Catalytic Walls at the Stagnation Region, 240,000 ft; 17,500 ft/sec

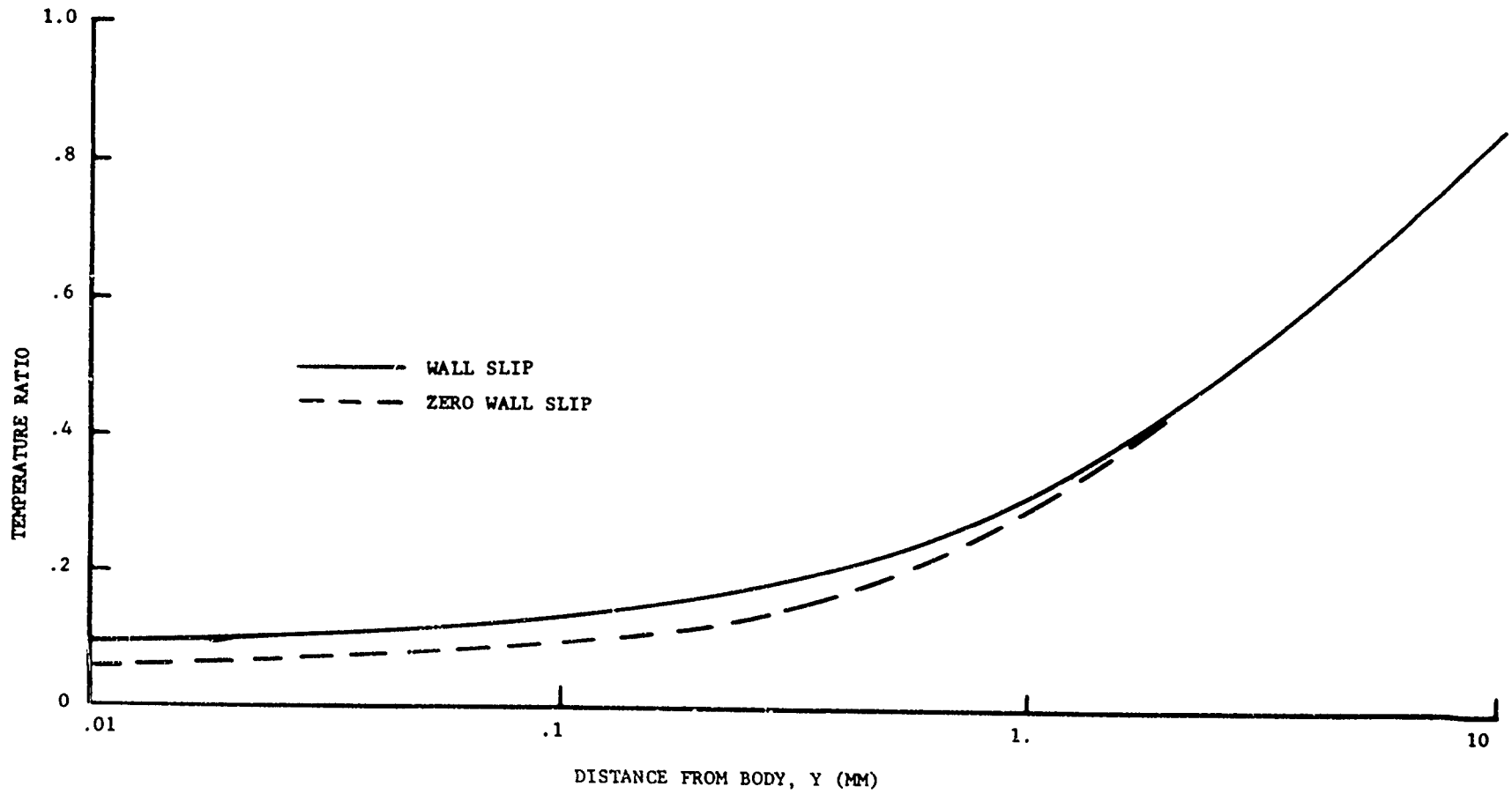


Figure 9. Effect of Wall Slip on the Temperature Distribution t the Stagnation Region, 270,000 ft; 17,500 ft/sec

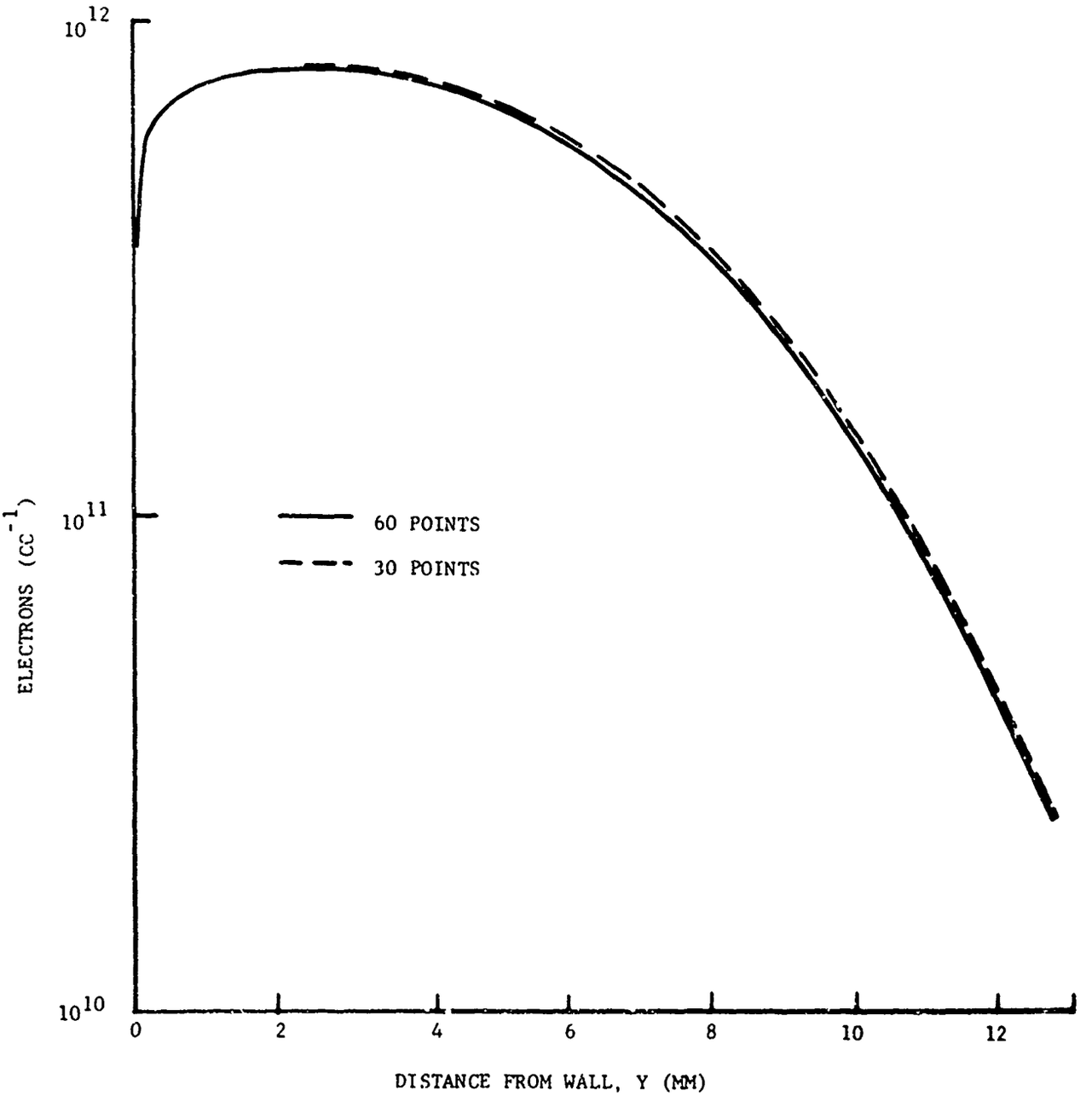


Figure 10. Effect of Step Size on the Distribution of Electron Density at the Stagnation Region for Vibrational Nonequilibrium, 240,000 ft; 17,500 ft/sec

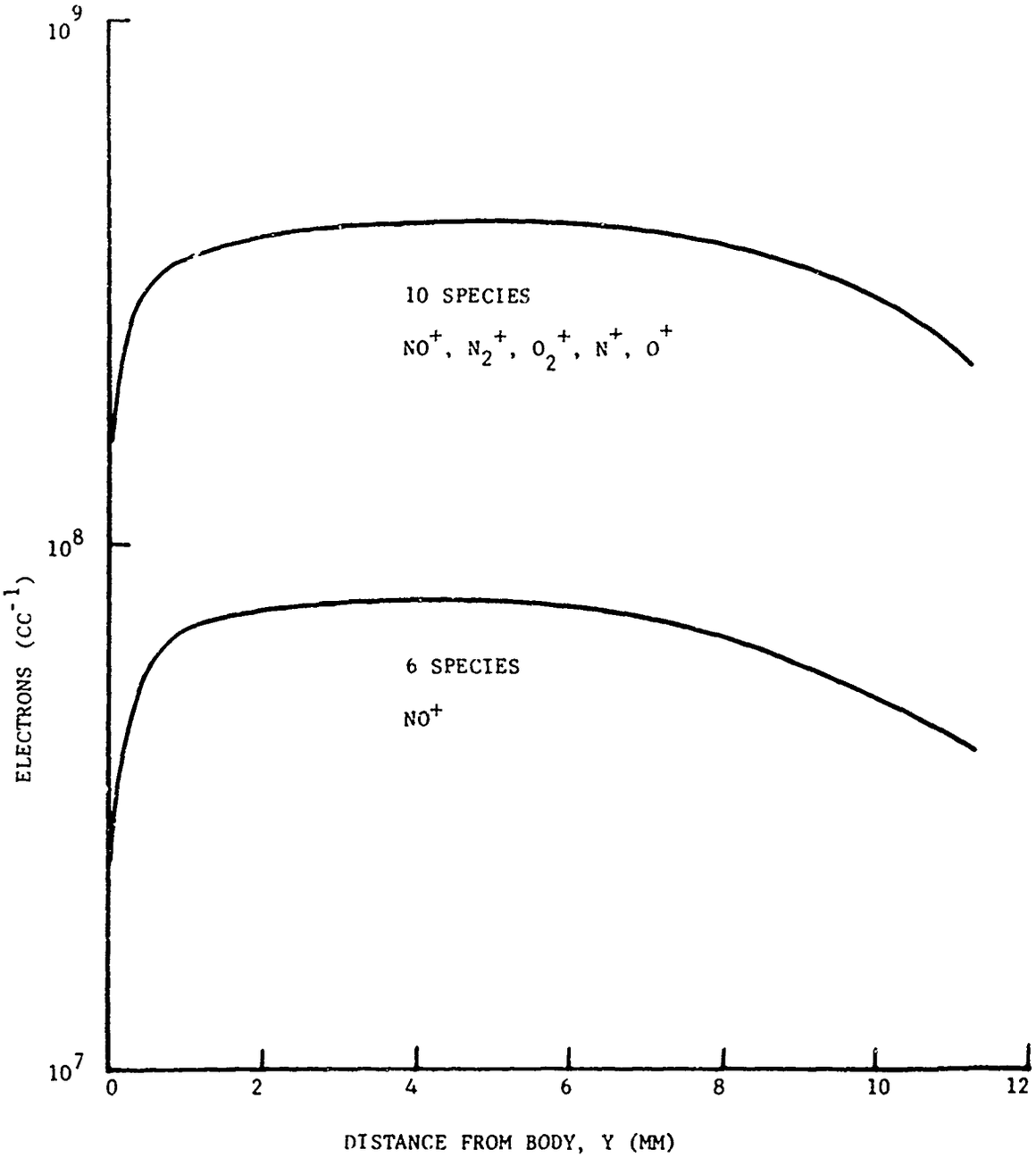


Figure 11. Electron Density Distributions at the Stagnation Region for 6 Species ($NO^+$) and 10 Species ($NO^+$, $N_2^+$, $O_2^+$, $N^+$, $O^+$) at 270,000 ft and 17,500 ft/sec

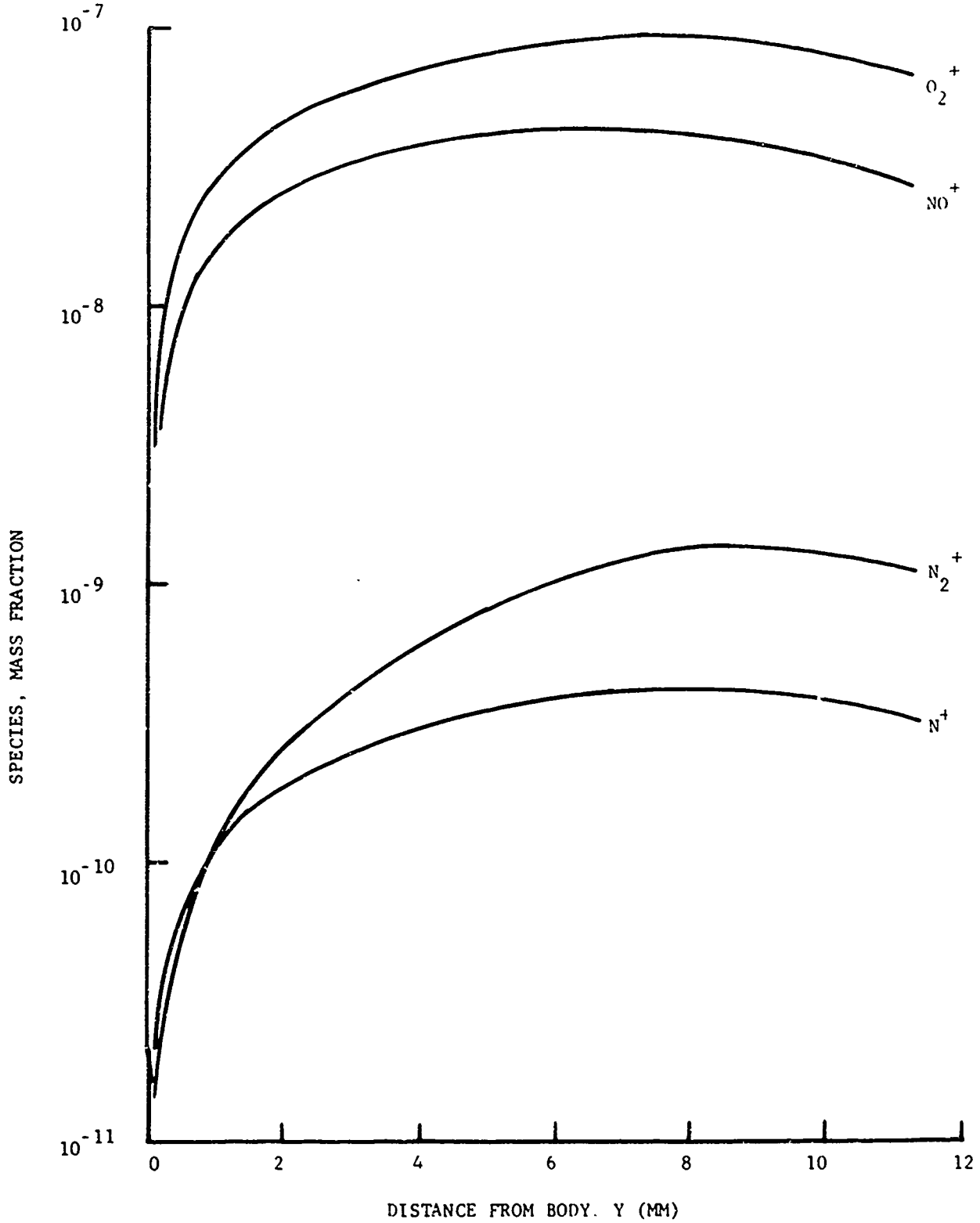


Figure 12. Ion Concentration at the Stagnation Region at 270,000 ft and 17,500 ft/sec

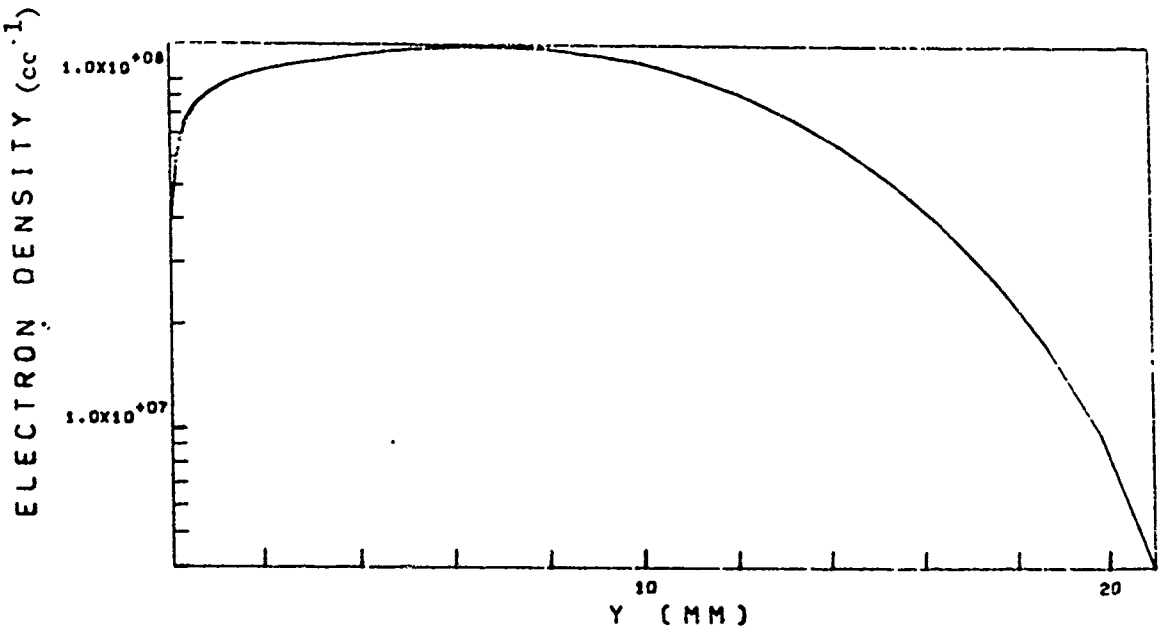


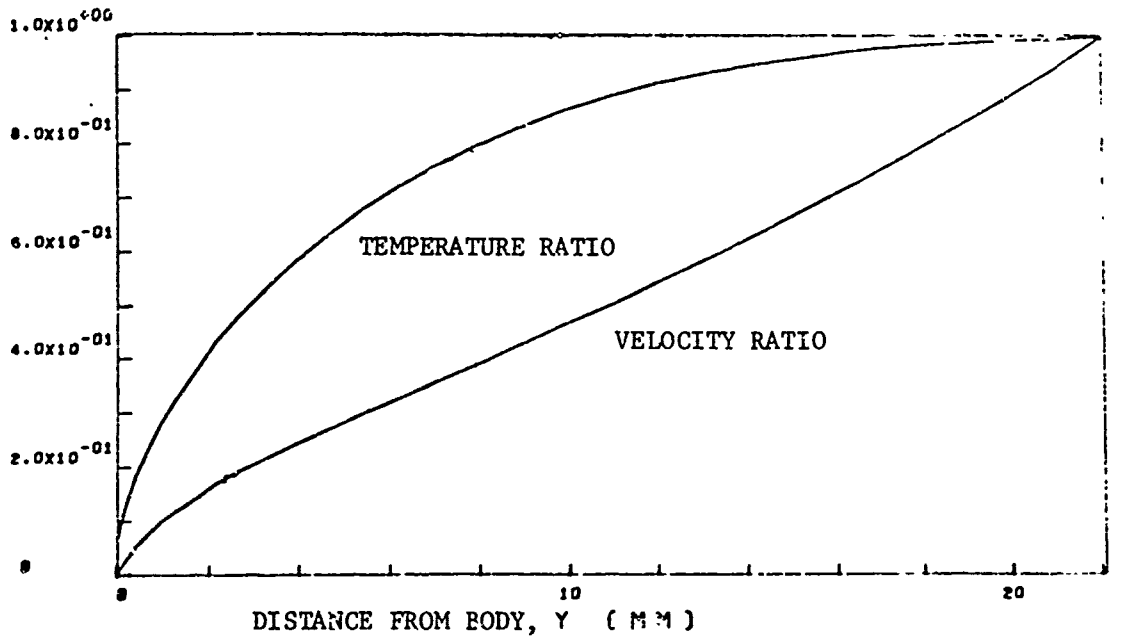


Figure 13. Temperature, Velocity, and Electron Density Profiles for the Sphere Cone Trailblazer Body at x = .066 meter, 270,000 ft; 17,500 ft/sec

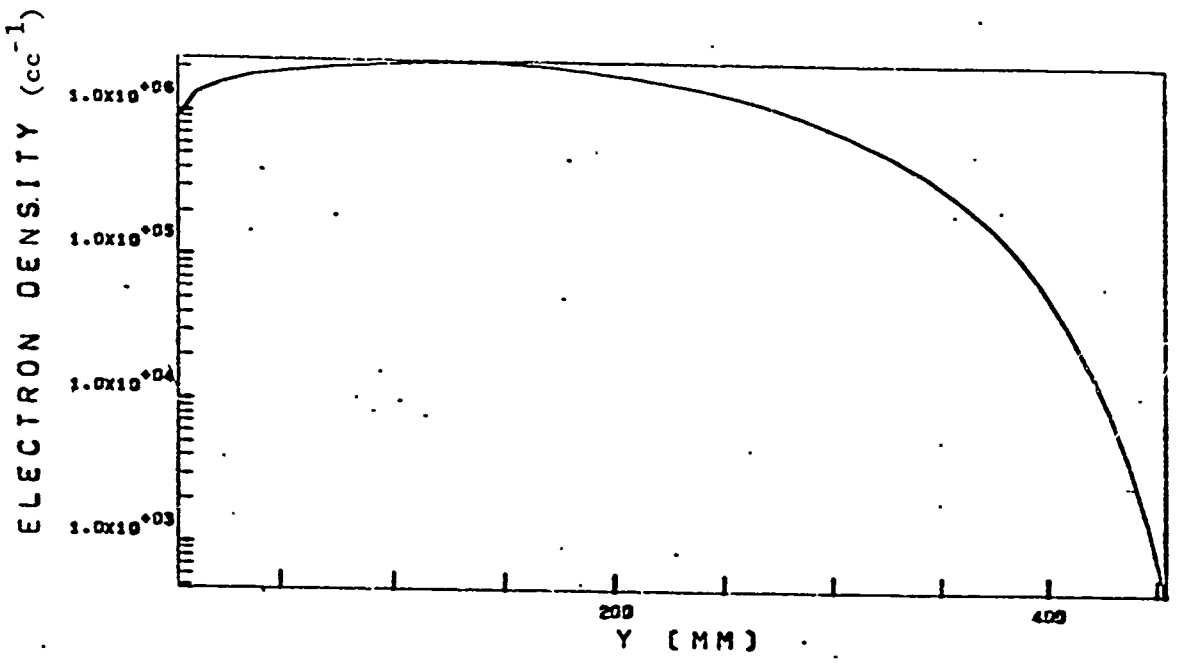


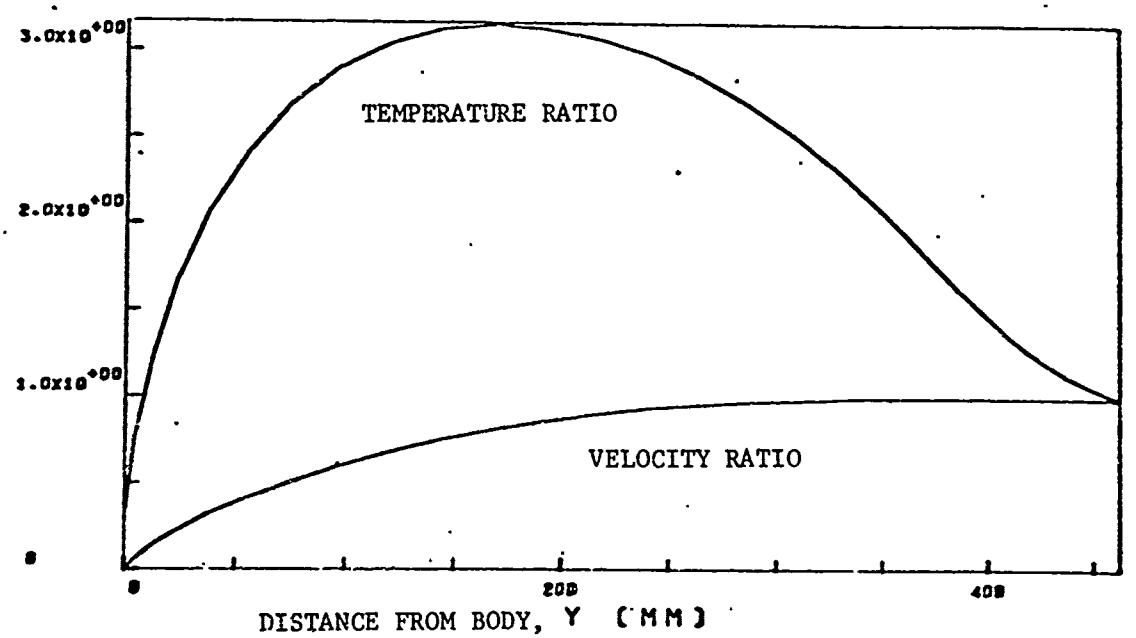


Figure 14. Temperature, Velocity, and Electron Density Profiles for the Sphere Cone Trailblazer Body at x = .066 meter, 270,000 ft; 17,500 ft/sec

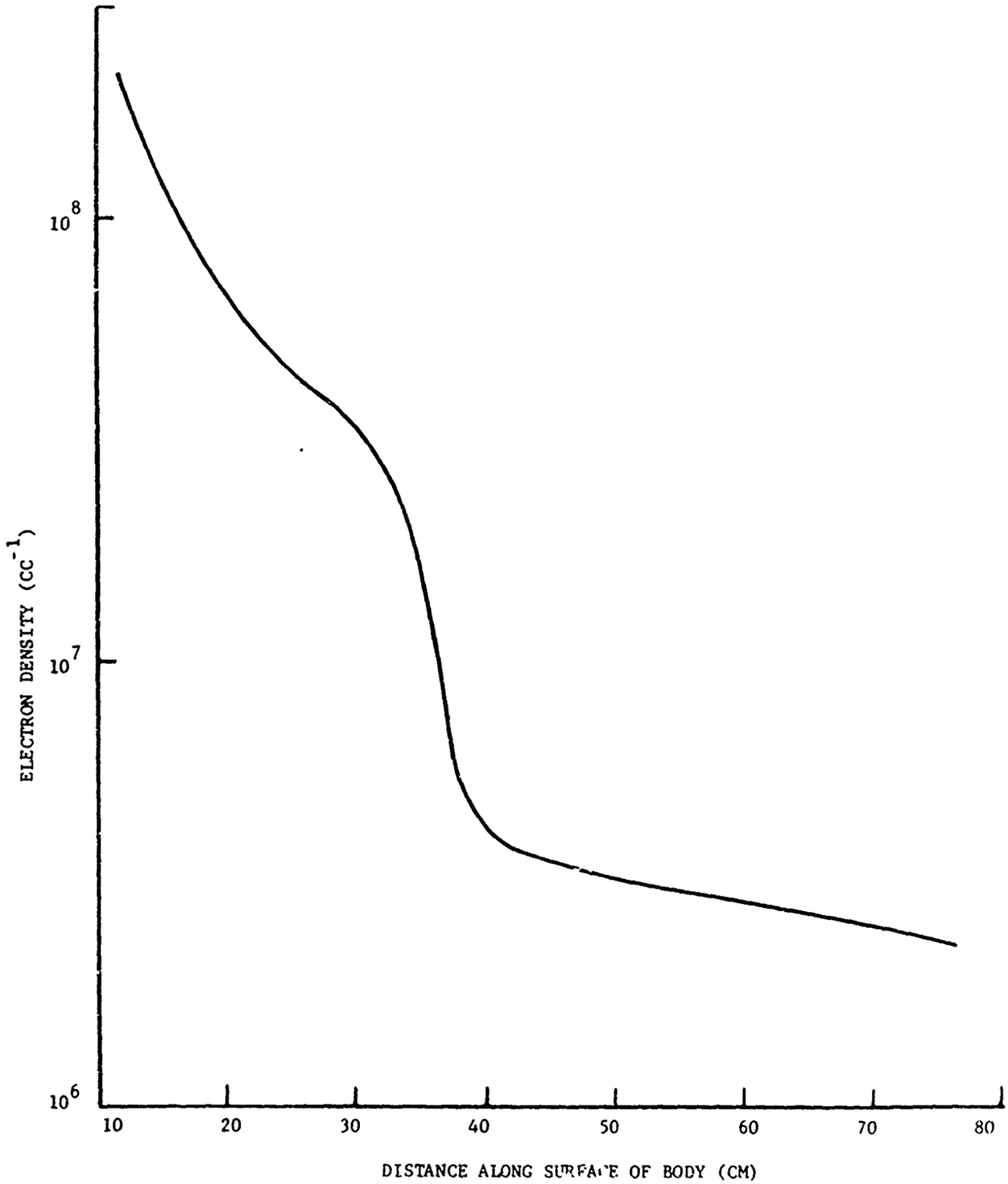


Figure 15. Peak Electron Density Decay Along the Body of Trailblazer at 270,000 ft and 17,500 ft/sec